JOURNAL OF MATERIALS SCIENCE **37** (2002) 3369–3375

# High-resolution elemental maps for three directions of $Mg_2Si$ phase in Al-Mg-Si alloy

K. MATSUDA*, T. KAWABATA
*Faculty of Engineering, Toyama University, 3190, Gofuku, Toyama, 930-8555, Japan*
*E-mail: matsuda@eng.toyama-u.ac.jp*

Y. UETANI
*Toyama Prefectural University, 5180, Kurokawa, Kosugi, Imizu, Toyama, 939-0389, Japan*

T. SATO
*Graduate School of Science and Engineering, Tokyo Institute of Technology, O-okayama, Meguro-ku, Tokyo, 152-8552, Japan*

S. IKENO
*Faculty of Engineering, Toyama University, 3190, Gofuku, Toyama, 930-8555, Japan*

Elemental maps of the Mg and Si sub-lattices of the $Mg_2Si$ phase in an Al-1.0mass% $Mg_2Si$ alloy were produced using an energy-filtering transmission electron microscope (EFTEM). Low magnification elemental maps were obtained using both low and high energy loss edges, and the intensities of the high energy loss edges were sufficiently high to allow the $Mg_2Si$ phase to be observed at high magnification. High-resolution core-loss images of Mg and Si-K edges were taken parallel to [001], [111] and [110] of the $Mg_2Si$ phase. In the [110] direction, Mg and Si atoms were successfully identified as sub-lattices. The Mg atoms formed a 0.39 nm diamond network, whereas the Si atoms formed a 0.32 nm by 0.22 nm rectangular network. This result is in good agreement with the projected potential of the $Mg_2Si$ phase in the [110] direction. This is the first report of magnesium and silicon atoms in the $Mg_2Si$ phase being successfully identified at the atomic level by EFTEM. 

## 1. Introduction

The development of high-resolution transmission electron microscope (HRTEM), which allows the lattice fringes of various materials to be observed directly, is recognized as a major advance in the research of phase decomposition and phase transformation in aluminum base alloys [1–3]. As HRTEM provides real space information for nano-scale regions in materials directly, rather than inverse space information as given by X-ray diffraction and electron diffraction techniques, the phenomena of phase decomposition and phase transformation at the atomic level has become easier for researcher to visualize. These developments in analytical transmission electron microscopy, however, have been somewhat overshadowed by the recent dramatic improvements in computer performance, quantitative software and the sensitivity of energy-dispersive X-ray spectroscopy (EDS). However, the specific structural and elemental arrangement of individual atoms cannot be observed by any of these methods, although nano-scale chemical compositions can be determined by EDS. EFTEM combines electron energy loss spectroscopy (EELS) with TEM, and is an excellent means of observing the precise chemical composition of materials [4]. A number of recent reports concerning the use of EFTEM to examine the chemical composition near the interfaces of semiconductor materials have been presented. Eibl [5], and Chang *et al*. [6] reported on the distribution of oxygen, silicon, nitrogen, titanium and aluminum in a 30 nm area using the jump-ratio (two-windows) method for very large scale integration (VLSI) material. Elemental maps are easier to produce by the jump-ratio method than by the three-windows method because image noise is low (high S/N ratio), and image acquisition is relatively quick [7, 8]. Hofer *et al*. [9] compared elemental maps produced by the jump-ratio method with those by the three-windows method for ODS-niobium. The three-windows method produces better elemental maps, however, the effect of diffraction contrasts cannot be removed from the final images perfectly. The jump-ratio method is convenient for use with samples of variable thickness or if bending may occur. The jump-ratio method, however, simply involves dividing a post-edge image by a pre-edge image. It has also been suggested that elemental maps produced by the three-windows method should be related to EDS and EELS data in order to explain obtained images. However, these previous studies were concerned

*Author to whom all correspondence should be addressed.

with 30 nm areas, and did not involve high magnification. Hence, it is unclear whether EFETM is useful for high resolution imaging, as is required for observing crystal lattices. An application EFTEM at high resolution for Si particles has been reported by Hashimoto *et al*. [10], however the technique has not yet to be applied to a binary system.

We have applied EFTEM analysis to commercial aluminum alloys, producing high-resolution core-loss images of magnesium and silicon atoms taken in the [001] direction of $Mg_2Si$ [11]. However at that time, there was a problem in that both magnesium and silicon atoms formed square networks of the same size. This made it difficult to determine whether a position in a unit cell was occupied by a magnesium atom or a silicon atom when the TEM specimen drifted during the recording of pre-edge 1, pre-edge 2, and post-edge images.

In this work, lattice fringes of the $\beta$-$Mg_2Si$ phase in an Al-Mg-Si alloy were observed by EFTEM and we have successfully obtained high-resolution maps for three crystal directions; [001], [111] and [110], of the equilibrium $Mg_2Si$ phase in Al-Mg-Si alloys. This intermetallic compound is conducive to EFTEM at high resolution, because the Mg or Si atoms form columns of a single element, which can be observed if the appropriate directions of the $Mg_2Si$-phase is chosen. It has also been confirmed that EFTEM is a useful way to distinguish between two elements in intermetallic compounds via lattice images.

## 2. Experimental procedure

The Al-1mass%$Mg_2Si$ alloy was made from ingots of aluminum (99.99%), magnesium (99.9%) and silicon (99.9%). An ingot obtained was hot- and cold-rolled to two kinds of sheets of 0.2 and 1.0 mm in thickness. These sheets were solution heated at 848 K for 3.6 ks and quenched in chilled water. The sheets were aged at 673 K for 3.6 ks. Samples of the $Mg_2Si$ phase for TEM were made by extraction using the thermal phenol method in the same way as detailed in our previous report [11]. The extracted $Mg_2Si$-phase was deposited on the micro-grid, supported by a copper mesh. Thin foils for TEM were also prepared by the electric polishing method. The EFTEM used was a JEOL 4010T with an energy-filtering system (Gatan, GIF-200). The accelerating voltage was 400 kV. This EFTEM was also equipped with an EDS (Noran, Voyager-4). The condenser and objective aperture diameters employed were both 70 $\mu$m, and the entrance aperture diameter of the GIF-200 was 3 mm. A zero-loss image was taken with an energy slit of 10 eV. Unfiltered high-resolution images were also taken and compared with the calculated images using the multi-slice method. The core-loss images of each element were taken by the three-window technique of the power-law model [7] using GIF software (EL/P), with an energy slit width of 30 eV. The following were chosen for the center of three windows for the Mg-K edge (energy offset = 1305 eV): Pre-edge 1 ($\Delta E_1$) = 1105 eV, pre-edge 2 ($\Delta E_2$) = 1205 eV, and post-edge ($\Delta E_3$) = 1345 eV. For the Si-K edge (energy offset = 1839 eV); $\Delta E_1$ = 1639 eV, $\Delta E_2$ = 1739 eV and $\Delta E_3$ = 1879 eV were used. The method used for background fitting was the power-law model. Spectra and images were recorded with a slow-scan CCD camera (1024 × 1024 pixel array) integrated within the GIF-200. High-resolution EFTEM images were recorded using a binning of 2 × 2 (512 × 512 pixels) and an exposure time of 30–60 s per window. The total time required to record a high-resolution core-loss image was therefore 90–180 s. The direct magnification to observe high-resolution images was 100,000× and the final magnification via GIF was 6,500,000×. When the intensities of the core-loss images were weak, they were converted to power spectrum patterns using Digital Micrograph software. The periodicity corresponding to the crystal structure of $Mg_2Si$ in these power spectrum (PS) patterns was selected by masking and the weak core-loss images were reconstructed using an inverse fast Fourier transform (IFFT) routine.

## 3. Results and discussion

A typical bright field image of the $Mg_2Si$-phase in an Al-1.0mass% $Mg_2Si$ alloy aged at 673 K for 3.6 ks is shown in Fig. 1a. The selected area diffraction pattern (SADP) shown in Fig. 1b, describes the [001] direction of the $Mg_2Si$, and has a lattice parameter of

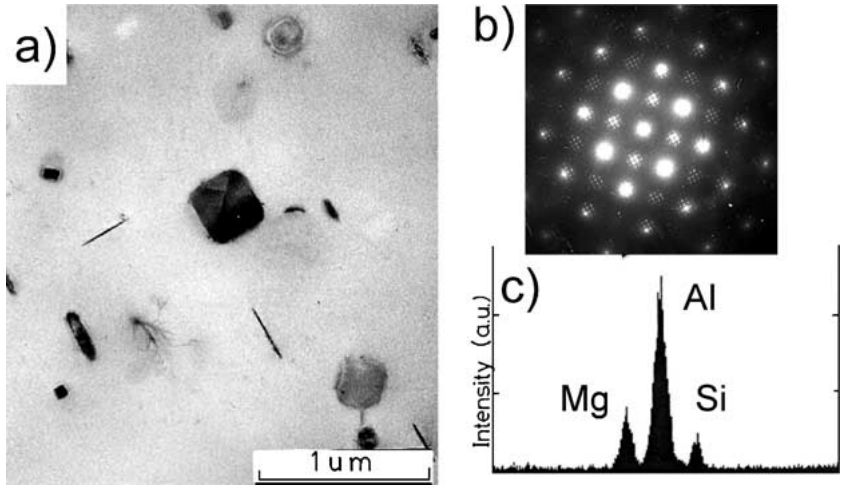


*Figure 1* (a) Typical bright field image of $Mg_2Si$-phase in Al-1.0mass% $Mg_2Si$ alloy aged at 673 K for 3.6 ks, and its (b) SADP and (c) EDS profiles.

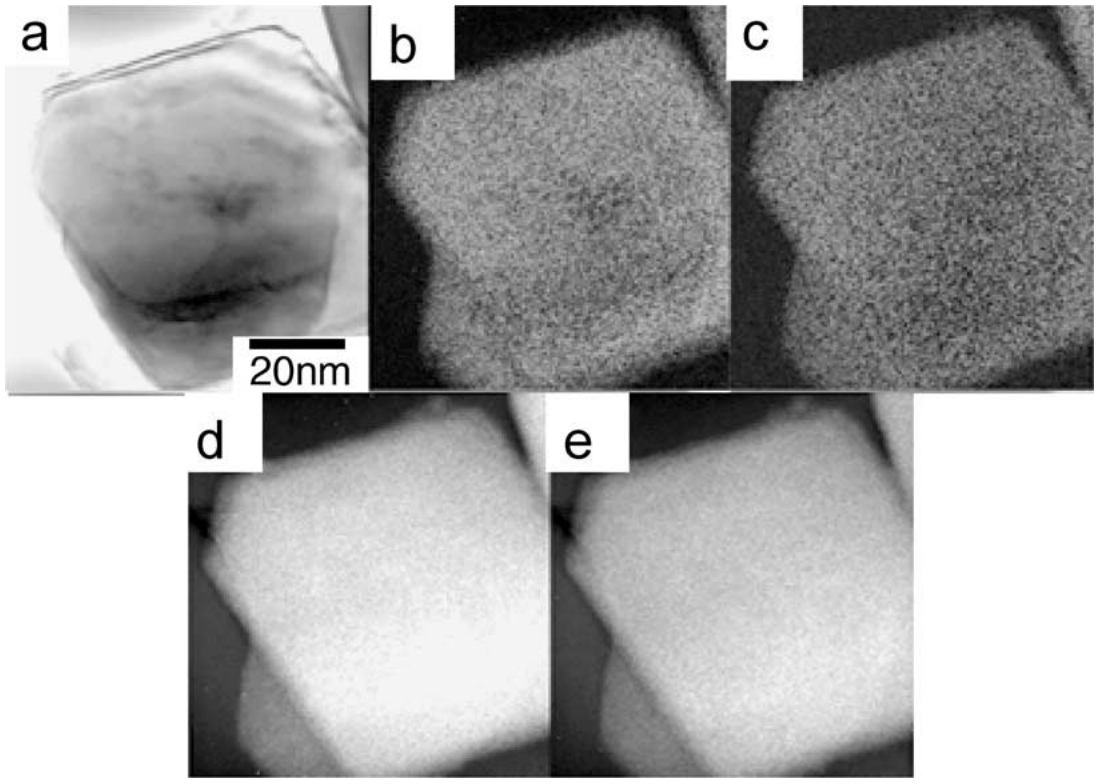


*Figure 2* EFTEM images of extracted $Mg_2Si$-phase, (a) zero-loss image and (b)–(e) core-loss images. (b) and (c) Core-loss images from high-loss edges of Mg and Si, and (d) and (e) from low-loss edges of Mg and Si.

$a = 0.635$ nm. The EDS profile exibits Mg, Al and Si peaks. As a high Al peak represents the matrix, the ratio of Mg to Si calculated from peaks of Mg and Si is about 2. The $Mg_2Si$-phase is plate-shaped, and its habit plane is known to be $[001]m//[001]\beta$ and $[100]m//[110]\beta$. The zero-loss image of the extracted $Mg_2Si$-phase is shown in Fig. 2a, and the corresponding EDS and EELS profiles are shown in Fig. 3. The EDS profile exhibits clear peaks due to Mg-Ka and Si-Ka, and the Mg/Si ratio is calculated to be about 2, which is consistent with previous reports [12].

The EELS profile has a sharp at both 1305 eV and 1839 eV, related to Mg-K and Si-K edges. The Mg/Si ratio calculated from these edges is about 2, which is in agreement with the EDS results. Core-loss images of the extracted $Mg_2Si$-phase shown in Fig. 2a were produced, as shown in Fig. 2b–e. Images produced from the high energy loss Mg-K and Si-K edges in Fig. 3b are shown in Fig. 2b and c. The intensities of these core-loss images by high loss edges are sufficiently high to allow the $Mg_2Si$-phase to be observed at high resolution, although the core-loss images produced from the low loss edges as shown in Fig. 2d and e are brighter than Fig. 2b and c. A high-resolution (HR) zero-loss image of the $Mg_2Si$-phase taken in the [001] direction is shown in Fig. 4a. Bright and dark dots arrange in a square network with a spacing of 0.32 nm. Fig. 4b is a schematic illustration of the projected potential of the $Mg_2Si$-phase in the [001] direction. Mg and Si atoms form columns consisting entirely of one or the other element in the [001] direction. The square networks of Mg and Si atoms with a spacing of 0.318 nm are shown in Fig. 4b. Our interest is which dots (bright or dark) in Fig. 4a correspond to Mg, and which to Si. To confirm this question, HR core-loss images were taken

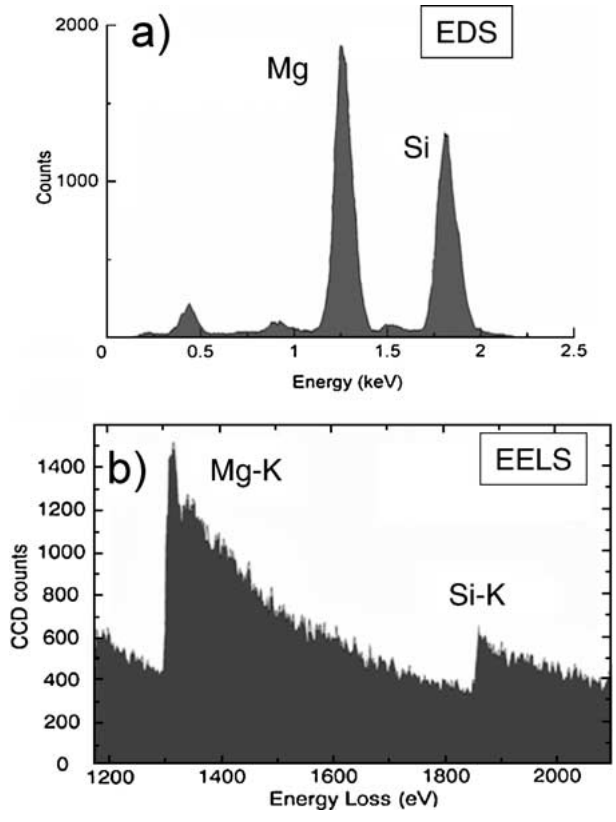


*Figure 3* Results of chemical analysis of $Mg_2Si$ phase. (a) EDS and (b) EELS profiles.

from the $Mg_2Si$ phase. Original HR core-loss images of Mg and Si are shown in Fig. 5a and b, respectively, in which square networks with a spacing of 0.32 nm can be seen. PS patterns were obtained from these core-loss images by the fast Fourier transforms (FFT). The images exhibit clear periodicities of the $Mg_2Si$ phase.

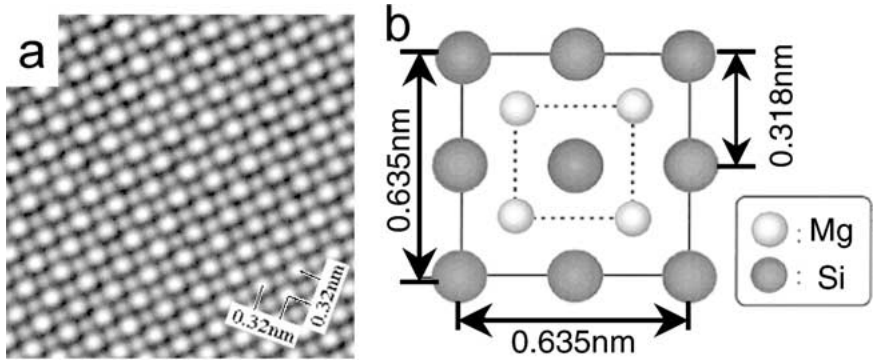


*Figure 4* (a) HR zero-loss image of $Mg_2Si$-phase in [001] direction. (b) schematic illustration of projected potential of $Mg_2Si$-phase in [001] direction.

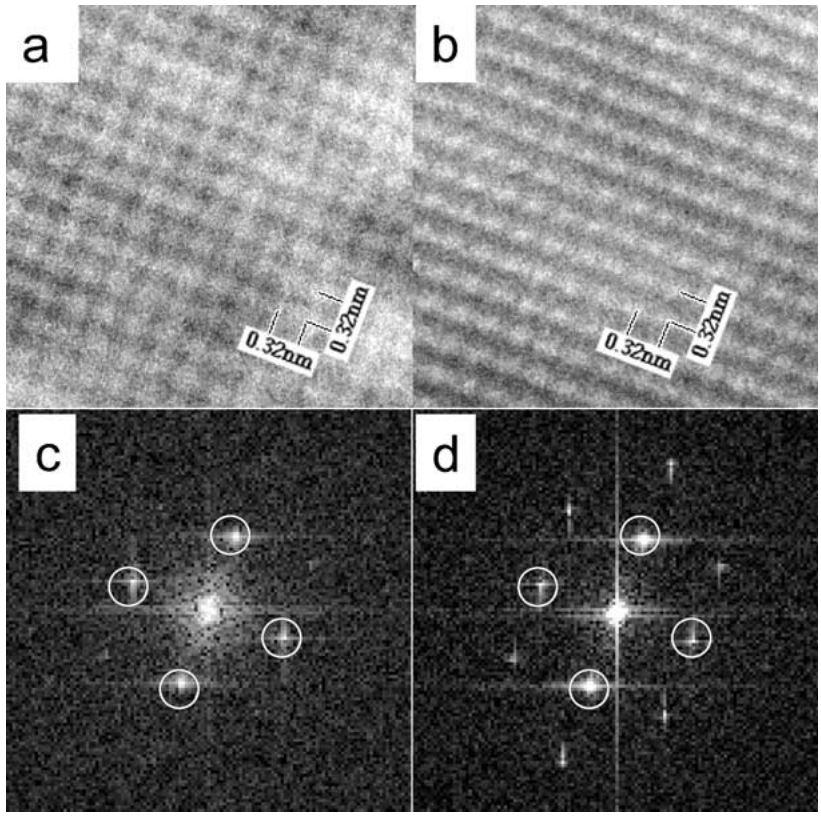


*Figure 5* (a) and (b) Original HR core-loss images of Mg and Si. (c) and (d) PS patterns from FFT of (a) and (b), respectively.

IFFT-HR core-loss images filtered with these FFT images are shown in Fig. 6a and b. The 0.32 nm square networks are clearer than Fig. 5c and d, and the atomic arrangements of Mg and Si sub-lattices in the $Mg_2Si$ phase can be distinguished. There is a possibility that the specimen may drift during analysis because it takes at least 3 minutes to make an elemental map for each element, and the specimen holder drifting during pre-edge 1, pre-edge 2 and post edge imaging, as well as during calculation.

HR core-loss images of the $Mg_2Si$ phase taken in the [111] direction reveal a typical superposition of atoms; Mg and Si atoms are superimposed in the [111] direction mutually and perfectly as shown in Fig 7b. The chemical composition of the atomic columns is 50% Mg. HR zero-loss image in Fig. 7a is in good agreement with a schematic illustration of the projected potential of the $Mg_2Si$-phase in the [111] direction in Fig. 7b, and shows triangular network having a spacing of 0.45 nm. The Mg and Si atoms in such triangular networks are not expected to be distinguishable in IFFT-HR core-loss images. IFFT-HR core-loss images for the two elements are are shown in Fig. 7c and d. As the two images show the same triangular arrangement of bright dots spaced at about 0.45 nm, the Mg and Si atoms can not be discriminated in the [111] direction.

The result of observation in the [110] direction is shown in Fig. 8. A diamond-shaped network of bright dots with a weak contrast between bright dots is seen in the HR zero-loss image in Fig. 8a. Two kinds of networks are present in the $Mg_2Si$-phase in the [110] direction as shown in Fig. 8b, namely a diamond-shaped network and a rectangular network. The former corresponds to Si atoms and latter one to Mg atoms and the two elements exist into these two columns similar to the [001] direction in Fig. 4b. The diamond-shaped network has a side length of 0.389 nm, and the rectangular network is 0.318 nm by 0.225 nm. A diamond-shaped network of bright dots can be seen clearly in Fig. 8a, and the weak contrasts corresponding to the rectangular

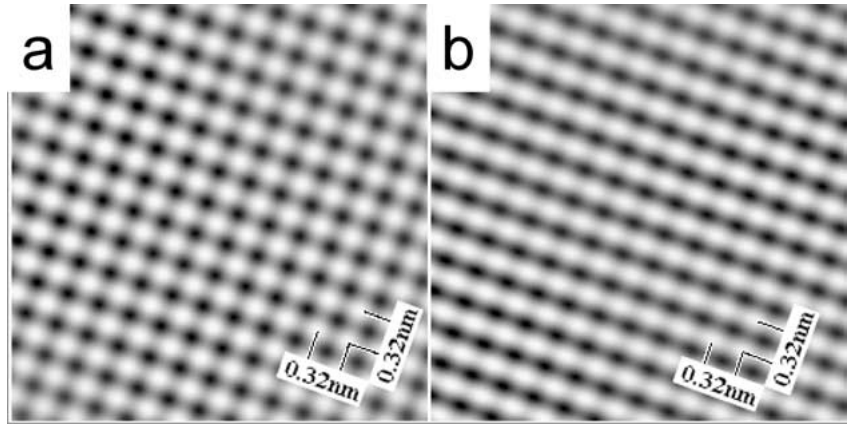


*Figure 6* (a) and (b) IFFT-HR core-loss images of Mg and Si filtered with Fig. 5c and d, respectively.

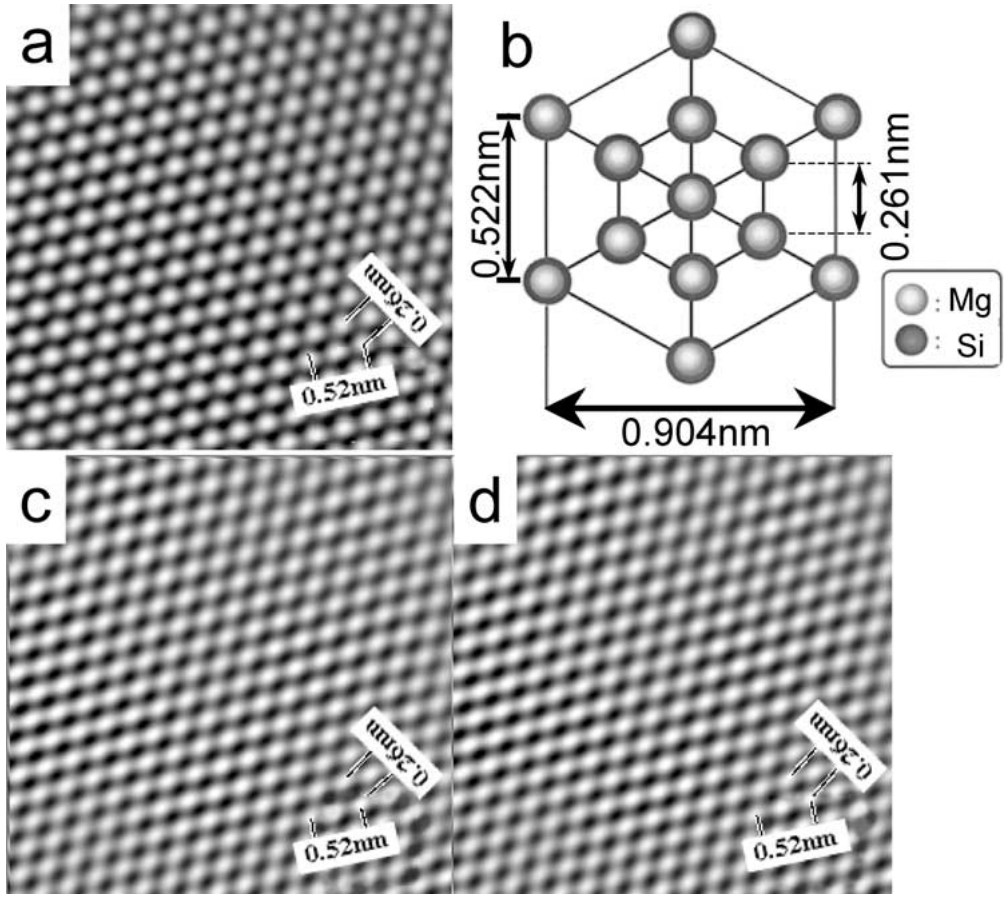


*Figure 7* (a) HR zero-loss image of $Mg_2Si$-phase in [111] direction. (b) schematic illustration of projected potential of $Mg_2Si$-phase in [111] direction. (c) and (d) IFFT-HR core-loss images of Mg and Si.

network can also be distinguished. IFFT-HR core-loss images of Mg and Si in the [110] direction are shown in Fig. 8c and d, respectively. The two elements have clearly different arrangements; Mg atoms form a rectangular network of dimensions 0.32 nm by 0.22 nm, and the Si atoms form a diamond-shaped network of sides 0.39 nm. This is in good agreement with the schematic illustration in Fig. 8b. This is the first report of Mg and Si atoms in the $Mg_2Si$ phase being successfully identified at the atomic level by EFTEM.

The spatial resolution $d$ by EFTEM is given by the following equation [4],

$$d = C_c\beta \cdot \Delta / E_0 \qquad (1)$$

where $C_c$ is the coefficient of chromatic aberration of the objective lens (1.4 mm), $\beta$ is the full angle as defined by the objective aperture (16 mrad), $\Delta$ is width of the energy slit (30 eV), and $E_0$ is the accelerating voltage (400 kV). Therefore, in this case, $d = 0.84$ nm. Kothleitner and Hofer [13] have used an equation of Krivanek *et al*. [14]:

$$d^2 = \left\{(2hv\theta_0/\mathrm{d}E)\cdot\left[(\theta_{0^2}+\theta_{E^2})\times\ln(1+(\theta_{0^2}/\theta_{E^2}))\right]^{-1/2}\right\}^2 + (C_c\Delta\theta_0/E_0)^2 + (0.6\lambda/\theta_0)^2 \qquad (2)$$

where $h$ is the Plank's constant, $v$ is the speed of the electron, $\theta_0$ is the maximum scattering angle admitted

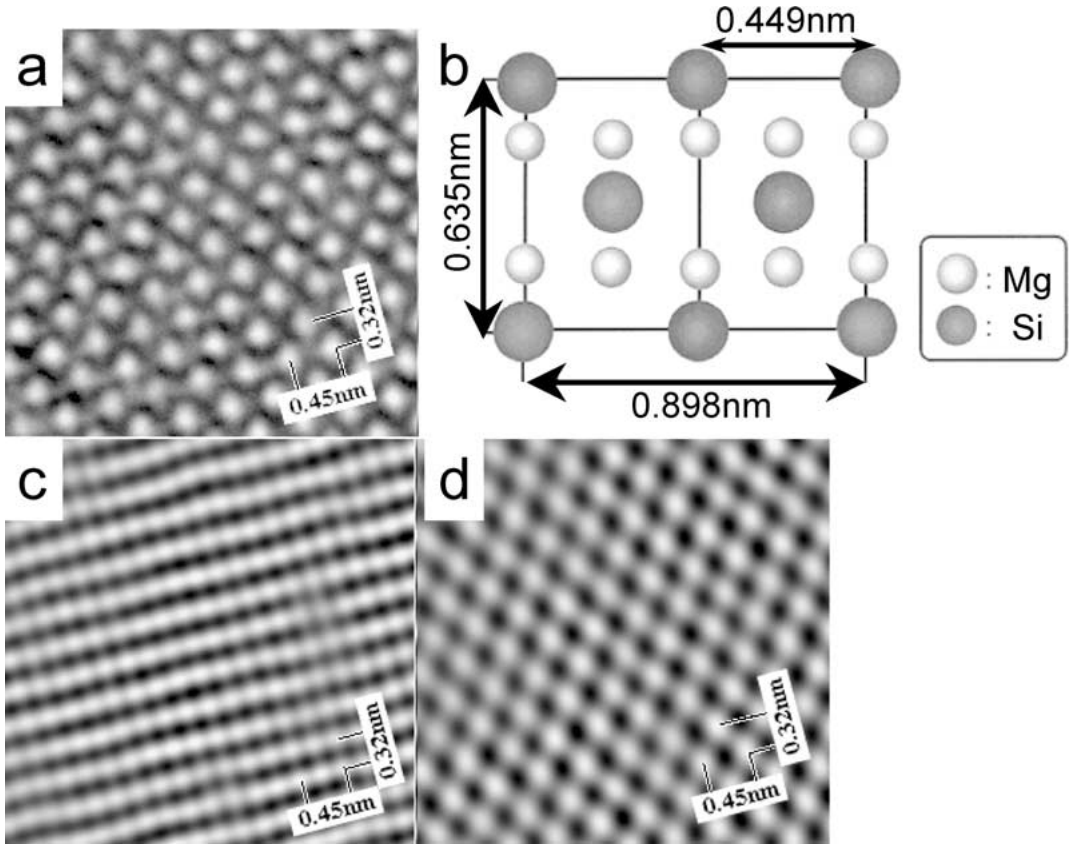


*Figure 8* (a) HR zero-loss image of $Mg_2Si$-phase in [110] direction. (b) schematic illustration of projected potential of $Mg_2Si$-phase in [110] direction. (c) and (d) IFFT-HR core-loss images of Mg and Si.

by the objective aperture, d$E$ is the energy loss, $\theta_E$ is $dE/E_0$, and $\lambda$ is the wave length of the electron. According to this equation, the spatial resolution of our EFTEM is 1.66 nm for the Mg-K edge at 1305 eV, and 1.08 nm for the Si-K edge at 1839 eV. This suggests that HR-EFTEM may be applicable to separating several kinds of elements in intermetallic compounds. In the present study we have realized higher resolution than these calculated resolutions, the cause of which is a subject of further investigation.

## 4. Concluding remarks

Mg and Si sub-lattices of the $Mg_2Si$ phase in an Al-1.0 mass% $Mg_2Si$ alloy were observed by EFTEM. The results obtained are summarized as follows:

1. Elemental maps of Mg and Si in the $Mg_2Si$ phase at lower magnification were obtained from both low-loss and high-loss edges of EFTEM. The intensities of elemental maps by high-loss energy edges were sufficiently high to allow observation of the $Mg_2Si$ phase at high magnification.
2. Chemical analysis of $Mg_2Si$ phase were preformed by EDS and EELS at the same time, and both results showed that the ratio of Mg to Si was about 2.0 as the same as previous reports.
3. HR core-loss images of Mg-K and Si-K edges were taken parallel to [001], [111] and [110] of the $Mg_2Si$ phase. In the [001] direction, both core-loss images of Mg and Si displayed square networks of 0.32 nm. Triangular networks of 0.45 nm were observed in the [111] direction however, sub-lattices of Mg and Si atoms could not be discriminated in this direction, as was expected from the projected potential of $Mg_2Si$ parallel to [111] direction. In the [110] direction, Mg and Si atoms were successfully identified in their respective sub-lattices. Mg atoms formed a diamond-shaped network of 0.39 nm, and Si atoms formed a rectangular network of 0.32 nm by 0.22 nm. This is in good agreement with the projected potential of $Mg_2Si$ phase in the [110] direction.

## Acknowledgements

The authors are grateful to the Hokuriku Fabrication Center, Shin-Nikkei Co. Ltd., for their chemical analysis of our alloys. This research was supported in part by the Saneyoshi foundation of Japan.

## References

1. R. W. FONDA, C. A. CASSADA and G. J. SHIFLET, *Acta Metall. Mater.* **40** (1992) 2539.
2. J. M. HOWE, U. DAHMEN and R. GRONSKY, *Phil. Mag.* A **56** (1987) 31.
3. K. MATSUDA, H. GAMADA, K. FUJII, Y. UETANI, T. SATO, A. KAMIO and S.IKENO, *Met. Mater. Trans.* A. **29A** (1998) 1161.
4. R. F. EGERTON, in "Electron Energy-Loss Spectroscopy in the Electron Microscope," 2nd ed. (Plenum Press, New York, 1996).
5. O. EIBL, *Ultramicroscopy* **69** (1997) 289.
6. H. CHANG, L. CHANG, F-.R. CHEN, J. J. KAI, E. TZOU, J. FU, Z. XU, J. EGERMEIER and F-.S. CHEN, *Acta Mater.* **46** (1996) 2431.
7. L. REIMER (ed.), in "Energy-Filtering Transmission Electron Microscopy" (Springer-Verlag, Berlin, 1995).

8. W. JAGER and J. MAYER, *Ultramicroscopy* **59** (1995) 33.
9. F. HOFER, P. WARBICHLER and W. GROGGER, *ibid.* **59** (1995) 15.
10. H. HASHIMOTO, *Bull. Electron Microscopy* **29** (1994) 68.
11. K. MATSUDA, T. NAOI, Y. UETANI, T. SATO, A. KAMIO and S. IKENO, *Scripta Mater* **41** (1999) 379.
12. I. J. POLMEAR, in "Light Alloys," 3rd ed. (Arnold, London, 1995) p. 39.
13. G. KOTHLEITNER and F. HOFER, *Micron* **29** (1998) 349.
14. O. L. KRIVANEK, M. K. KUNDMANN and K. KIMOTO, *J. Microscopy* **180** (1995) 277.

*Received 5 December 2001*
*and accepted 23 April 2002*